Perturbation of the mitochondrial import machinery by disease prone Tau affects organelle morphology and reduces neuronal complexity

Hope I Needs, Jeremy M Henley†, Ian Collinson†

School of Biochemistry, University of Bristol, Bristol BS8 1TD, UK

†, corresponding authors: ian.collinson@bristol.ac.uk and J.M.Henley@bristol.ac.uk

Abstract

Protein import into mitochondria is an intricate and highly conserved process essential for organellar biogenesis, and maintenance of its structure and function. Defects in the import apparatus impact the assembly of the respiratory chain and ATP synthase complexes required for oxidative phosphorylation, compromising the ready supply of ATP to the cell. The consequences of reduced bioenergetic function are particularly severe for cells with high energetic demands such as neurons. However, relatively little is known about how defective import contributes to neurodegeneration, or how neurotoxic proteins characteristic of neurodegenerative diseases impact mitochondrial import efficiency. Here, we used HeLa cells to investigate how expressing high levels of Tau variants affect mitochondrial import activity, morphology, and function. We found that the variant associated with neurodegeneration (Tau^{P301L}) colocalises with mitochondria. Tau^{P301L}, but not wildtype Tau, interacts with TOM40, the protein-channel component of the outer membrane protein import complex. Interestingly, Tau^{P301L} expression had no discernible effect on overall mitochondrial import function, despite associating with TOM40 and altering mitochondrial morphology, suggesting that a rescue mechanism is at play. This rescue could be explained by the appearance of microtubule and actin containing tunnelling nanotubes (TNTs), used to recruit healthy mitochondria from neighbouring cells and/or dispose of mitochondria with aggregated Tau. Furthermore, in primary neuronal cultures Tau^{P301L} induces morphological changes that resemble a neurodegeneration like phenotype, and this is mirrored in cells where the import sites are blocked artificially. These results reveal an intriguing link between the production of aggregation prone protein variants, such as Tau, and the mitochondrial protein import machinery relevant to neurodegenerative disease.

Introduction

Mitochondrial protein import is a highly conserved process by which most mitochondrial proteins are transported from the cytosol, where they are synthesised, *via* highly specialised import pathways, to their correct localisation within the mitochondrion. The translocase of the outer membrane (TOM) complex acts as the central entry gate for precursor proteins to enter the intermembrane space (IMS), where proteins then disperse into individual pathways, depending on their structure, function, and target destination [1]. The TOM complex consists of assembly/stability subunits (TOM5, TOM6, and TOM7), receptor subunits (TOM20, TOM22, and TOM70), and a central pore forming subunit (TOM40) [1, 2]. The presequence pathway is used by precursor proteins with cleavable N-terminal mitochondrial targeting sequences (MTS). These proteins are either laterally inserted into, or transported across, the inner mitochondrial membrane (IMM) *via* the translocase of the inner membrane sort ($TIM23^{SORT}$) or motor ($TIM23^{MOTOR}$) complexes, respectively. Cleavage of the MTS enables the folding and release of the mature protein [1].

These pathways (recently reviewed in refs. [3-5]) need to be tightly regulated and quality controlled to maintain mitochondrial structure and function, required for the supply of energy (ATP), cellular homeostasis, and overall health [6]. Mitochondrial dysfunction is one of the hallmarks of neurodegeneration, which is increasingly showing links to protein import machinery failure [7, 8]. For example, mitochondria from Alzheimer's patient brains accumulated amyloid precursor protein (APP), through the formation of stable complexes with protein channel components of the outer and inner membranes: TOM40 and TIM23 [9]. Similarly, mitochondria isolated from the brains of people affected by Huntington's disease were decorated with the aggregation prone variant of the Huntingtin protein (Htt). Again, Htt associates with the TIM23 complex and was shown to inhibit import as a result [10].

Neurofibrillary tangles (NFTs) comprise insoluble aggregations made up primarily of hyperphosphorylated Tau protein. NFTs are characteristic of Alzheimer's disease, as well as of all other primary and secondary tauopathies [11]. Tau is highly abundant in neurons and is mostly localised to the axons, where it binds to microtubules: promoting their assembly and stability [12-14]. Upon binding to microtubules, Tau modulates the activity of motor proteins Dynein and Kinesin, which in turn regulates the axonal transport of cargo including mitochondria [15-19]. However, the ability of Tau to bind microtubules is a highly dynamic process and is dependent on different Tau isoforms, mutations, and post-translational modifications. Due to the vital role of Tau in axonal migration, its aberrant behaviour can bring about neurological pathogenesis [20-23]. The Tau^{P301L} variant is commonly found in patients

with tauopathies and has been well characterised in disease models [24, 25]. Tau^{P301L} is known to have an increased propensity to form NFTs [26].

Mitochondrial function is impaired by abnormal, pathological Tau, but the mechanism is not yet fully understood. The accumulation of Tau into NFTs can elicit a number of specific mitochondrial effects. These include increased retrograde transport of mitochondria (*i.e.*, towards the soma); reduced complex I activity, ATP levels, and membrane potential; enhanced oxidative stress; and defective mitophagy [19, 27-29]. Furthermore, various studies have shown that aggregation prone Tau accumulates within the IMS and OMM [29, 30]. Tau mitochondrial accumulation and alterations in membrane potential suggest that there may also be import defects, since membrane potential is required for translocation of proteins across the IMM. However, no studies have yet directly associated import defects with pathological Tau.

Here, we show that the disease associated Tau^{P301L} variant interacts with the channel forming subunit of the TOM complex (TOM40). This interaction does not occur with the native form of Tau. Tau^{P301L} association with TOM40 corresponds to changes in mitochondrial morphology together with a reduction of neuronal complexity – consistent with neurodegeneration. Interestingly, the changes in neuronal structure were also induced when the mitochondrial import sites were artificially blocked. This suggests that perturbation of mitochondrial protein import, specifically by blockage of the TOM channel by variants of Tau or other aggregation prone proteins, may be an important factor in the onset of neurodegenerative diseases.

Results

The aggregation prone variant Tau^{P301L} associates with the mitochondrial import machinery

We investigated the association of Tau variants with mitochondria in HeLa cells conditioned with galactose (HeLaGAL), which impairs glycolytic metabolism and drives cells to be more dependent on mitochondria for their energy supplies. We carried out Western blotting analysis on mitochondrial and cytosolic fractions isolated from these cells over-producing Myc-Tau^{WT}, Myc-Tau^{P301L}, or a GFP only control (Fig. 1A, left panel). The results show that, in Myc-Tau^{P301L} containing cells, there was a higher proportion of the Tau protein localised to mitochondria compared to those expressing Myc-Tau^{WT} or GFP (Fig. 1A, left panel –quantified in 1B). To test whether the increased mitochondrial localisation of Tau^{P301L} correlates with altered import pathways, we expanded this analysis to include a selection of subunits of the import machinery (Fig. 1A, right panel –quantified in 1C). Overall, mitochondria from cells overexpressing

Tau^{P301L} had lower levels of mitochondrial TOM20 (receptor subunit of TOM40 complex localised in the OMM) and TIM23 (channel forming subunit of the TIM23 complex in the IMM) compared to control cells, but there was no change in TOM40 (channel forming subunit of TOM40 complex of the OMM) abundance. Together, these data are indicative of mitochondrial import defects induced by Tau^{P301L}.

Next, we investigated the interaction between Tau^{P301L} and the translocation machinery of the presequence pathway. We used Myc-trap pull-down assays on mitochondria isolated from cells producing recombinant Myc-GFP, Myc-Tau^{WT}, or Myc-Tau^{P301L}. Western blots showed that Tau^{P301L}, but not its native counterpart or the GFP control, associates with TOM40, but not TIM23 or TOM20, in the mitochondria of HeLaGAL cells (Fig. 1D and S1). This is consistent with previous reports which showed Tau^{P301L} accumulation in the OMM and IMS [29, 30], and suggests that it may be associated with the translocation channel in a similar way to an artificially trapped precursor protein [31, 32] (Needs *et al.* BioRxiv, November 2022). Surprisingly, despite association of Tau^{P301L} with the import machinery, the import kinetics of a precursor reporter were not significantly affected (Fig. 1E and S2).

Analysis of mitochondrial branching showed that cells expressing Tau^{P301L} have significantly fewer branches per mitochondrial network on average, when compared to mitochondria from cells expressing Tau^{WT} or GFP (3.9 compared to 5.9 and 6.6, respectively; Fig. 1F, G). The maximum number of branches per network is also reduced to 127.3 for Tau^{P301L}, compared to 276.9 for Tau^{WT} and 298.3 for GFP (Fig. 1H). Analysis of respiratory function *via* mitochondrial stress tests and membrane potential by measurement of TMRM fluorescence showed that, despite alterations in mitochondrial morphology, there was no change in the respiratory capacity (Fig. S3) or membrane potential (Fig. S4) in cells overexpressing Tau variants.

Tau^{P301L} overproduction induces TNT formation

In a parallel study, we explored the effects of artificially blocking the import machinery (Needs *et al.* BioRxiv, November 2022). This can be achieved with a precursor fused to DHFR, which when bound to methotrexate becomes trapped in the channel [31, 32], or with a small molecule inhibitor MB20 [33]. While these treatments inhibit import in isolated mitochondria, unexpectedly we found that they fail to do so within intact cells (Needs *et al.* BioRxiv, November 2022). We wondered if the apparent lack of effect on the whole mitochondrial population of the cell could be explained by a mitochondrial replacement system. We found that, at the whole cell level, defective mitochondrial function is rescued by the recruitment of healthy mitochondria from surrounding cells, and disposal of compromised mitochondria, *via*

TNTs (Needs *et al.* BioRxiv, November 2022). Therefore, we were curious if the association of the Tau variant to the import apparatus induced a similar response.

HeLa cells co-expressing mCherry with either Myc-GFP, Myc-Tau^{WT}, or Myc-Tau^{P301L} were analysed by confocal microscopy. The results show that in cells conditioned with galactose, which are dependent on mitochondrial ATP production, expression of the aggregation prone Myc-Tau^{P301L} induced TNTs: 62% of all cells exhibited TNTs, compared to 20% of cells producing native Tau (Fig. 2A, B). Glycolytic cells, cultured in glucose containing media, were significantly less prone to TNT production. The formation of TNTs could explain why the association of Tau^{P301L} with import machinery has no impact on protein import activity: *via* a TNT-dependent rescue mechanism to replace defective mitochondria. Consistent with this hypothesis, we observed mitochondria inside the TNTs (Fig. 2C), potentially on their way to rescue Tau affected cells.

The TNTs induced by precursor trapping contain actin as well as microtubules, necessary for mitochondrial movement along them (Needs *et al.* BioRxiv, November 2022). Thus, drugs that target actin (cytochalasin D) and tubulin (nocodazole) polymerisation inhibit TNT formation [34-36]. The TNTs induced here also contain actin and tubulin and their drug response is the same (Fig. 2D and S5). Therefore, perturbation of the import machinery by precursor trapping, small molecule inhibition, and aggregation with Tau all seem to induce a common response involving TNTs.

The overproduction of Tau^{P301L} and precursor trapping both bring about reduced neuronal complexity

Next, we explored the effects of perturbing the mitochondrial import machinery in neurons. In particular, we wanted to compare the effects of precursor trapping (deploying a precursor-DHFR fusion in the presence of MTX) against production of Tau^{P301L} in primary neurons. We used confocal microscopy to assess neuronal morphology of DIV21 primary hippocampal neurons following 7 days of precursor trapping or Tau variant overexpression. DIV21 neurons equate to 'mature' neurons with spines and fully formed synapses [37, 38] and therefore allow analysis of synapses and neuronal complexity. Axons are identified by staining for Ankyrin G, a scaffolding protein important in formation of the initial segment of the axon [39].

Overproduction of native Tau caused a significant reduction in the number of processes per cell compared to the GFP control (Fig. 3A, B; Tau^{WT}). Expression of the aggregation prone Tau^{P301L} caused a more pronounced reduction in processes (Fig. 3A, B; Tau^{P301L}). Interestingly, despite the reduction in neuronal complexity, neither Tau variant affected axonal

length (Fig. 3C). To determine if these effects were attributable to perturbation of the import machinery by Tau, we also subjected primary neurons to mitochondrial precursor trapping. Inclusion of the precursor alone did not affect cell complexity but when the import of this precursor was stalled by MTX addition, the number of processes was significantly reduced (Fig. 3D, E): mirroring the effect of Tau. In addition, however, stalling import significantly reduced axonal length (Fig. 3F; +MTS, +MTX), suggesting a more severe response. Importantly, the changes in length and complexity were not due to non-specific effects of MTX, as they are dependent on the MTS (Fig. 3E, F; -MTS, ±MTX), and neuronal viability was unaffected by precursor trapping or production of Tau variants (Fig. S6).

The results indicate that a reduction in neuronal complexity and length is brought about by perturbation of the protein import machinery. Notwithstanding the differing response to axonal length, this morphological change can be induced either by artificial precursor stalling, or Tau^{P301L} association with the TOM40 import channel, which we propose is mediated *via* a common mechanism.

Precursor trapping and Tau^{P301L} correlate with fewer synapses

The neuronal analysis was expanded to investigate the number of synapses per dendrite. PSD95 is the major scaffold protein involved in the organisation of postsynaptic signalling complexes in excitatory neurons [40]. These signalling complexes comprise glutamate receptors, ion channels, signalling enzymes and adhesion proteins, and are therefore vital in neurotransmission [41]. PSD95 is commonly used as a marker of excitatory (glutamatergic) post-synapses, due to its high abundance.

In neurons containing Tau^{P301L}, there was an average of 1.8 synapses per 10 µm dendrite, significantly lower than cells expressing GFP or native Tau, both of which had about twice as many (Fig. 4A, B). Subsequent Western blotting analysis determined that there was no change in the overall abundance of PSD95, Gephyrin, or Synaptophysin in whole cell lysates from cortical cells expressing GFP, or either of the Tau variants (Fig. S7). This indicates that the reduction in PSD95 expression at dendritic spines, *i.e.,* synapse abundance, is due to a change in the localisation of synaptic proteins and subsequent synapse assembly, rather than a reduction in the proteins' overall cellular abundance.

Perturbation of the import machinery by precursor trapping induced an almost identical reduction in the number of synapses per dendrite (Fig. 4C, D). Again, the controls show that synaptic loss is correlated to the precursor trapping and not MTX treatment, since in the absence of a presequence (-MTS) there is no significant change in the number of synapses

in the presence of MTX (Fig. 4D, -MTS, ±MTX). Western blotting analysis showed that the overall cellular abundance of all three synaptic marker proteins remained constant irrespective of precursor trapping (Fig. S8); as noted above for the Tau variants.

Discussion

This study explores aspects of the mitochondrial, cellular, and specific neuronal responses to Tau overexpression, specifically aggregation prone Tau^{P301L} that is implicated in neurodegeneration. We established that association of Tau^{P301L} with mitochondrial protein import machinery correlates with disease-like phenotypic changes in mitochondria and neurons. Moreover, the effects of Tau mirror those elicited by a precursor protein artificially stalled within the import machinery by a C-terminal fusion of DHFR bound to methotrexate (MTX).

At the mitochondrial level, there are profound morphological changes with decreased branching (Tau aggregation) and increased fission (precursor trapping) (Needs *et al.* BioRxiv, November 2022). Unexpectedly, however, neither Tau^{P301L} nor precursor trapping affected overall mitochondrial import activity. We postulate that this can be explained by the fact that both Tau^{P301L} and precursor trapping induced the formation of actin and tubulin containing tunnelling nanotubes (TNTs) (Needs *et al.* BioRxiv, November 2022). It has been shown in a number of previous studies that TNTs can provide a conduit for exchange of mitochondria between cells (summarised in a recent review [42]). Thus, we propose that healthy mitochondria are recruited to damaged cells *via* TNTs from nearby unaffected cells, and damaged mitochondria are likely disposed of *via* the same route, as we recently showed with precursor trapping (Needs *et al.* BioRxiv, November 2022). This process could also provide a rescue mechanism that explains the observed preservation of whole cellular mitochondrial import activity and respiratory function despite Tau^{P301L} accumulation within the TOM40 import channel.

The Tau induced neuronal changes recapitulate those seen by precursor trapping. These data strongly suggest that they act *via* perturbation of the import machinery. In this context, we do not yet know if the rescue response, noted in mitochondria dependent HeLa cells, involving TNTs is deployed. The decrease in processes and synaptic density, induced by perturbation of the import machinery, are consistent with neurodegeneration. Therefore, an important future goal is to determine if the rescue mechanism is implemented in neurons, and if so to what extent it mitigates against more severe neuronal aberrations, or cell death.

The variant Tau^{P301L} has been extensively characterised [24-26], and in agreement with the results shown here, it has previously been shown to localise at the mitochondrial IMS and OMM [29, 30]. However, its interaction with translocation machinery had not previously been reported. Nonetheless, its association with mitochondrial translocases is reminiscent of that observed for other proteins implicated in neurodegeneration, such as APP, Huntingtin, and alpha-synuclein [9, 10, 43]. Therefore, the neuronal effects of import perturbation shown here point to a common mechanism that could be an important underlying factor in multiple neurological diseases. Indeed, recent reports have linked failed import or aggregation of proteins within import sites with neurodegenerative diseases: both aggregation prone APP and the Huntingtin protein variant become trapped in import sites and are directly correlated with mitochondrial dysfunction [9, 10].

The exact mechanism linking import perturbation and the neuronal irregularities, including the role of TNTs and rescue, remain unclear. Nevertheless, the evidence suggests that our artificial trapping substrate is indeed mimicking what is seen in disease. Therefore, it provides us with a useful tool to explore within cell cultures and in model organisms, to better understand import dysfunction as a potential contributory factor in the onset of neurodegenerative disease. Moreover, deeper analysis of the potential TNT-mediated rescue mechanism will be interesting with regards to early and late onset neurodegeneration, and perhaps how the timing could be delayed.

Acknowledgments

We gratefully acknowledge access and support of the Wolfson Bioimaging Facility. We acknowledge Dr Stephen Cross and Dr Richard Seager for image analysis support. We acknowledge Dr Kevin Wilkinson for kindly gifting constructs. We acknowledge the University of Bristol Animal Services Unit for animal support.

Funding

This work was funded by the Welcome Trust: to HIN through the Wellcome Trust Dynamic Molecular Cell Biology PhD programme (083474) and IC by a Wellcome Investigator award (104632).

The funders had no role in study design, data collection and interpretation, or the decision to submit the work for publication. For the purpose of Open Access, the authors have applied a CC BY public copyright license to any Author Accepted Manuscript version arising from this submission.

Author contribution

HIN, JMH and IC designed experiments; HIN conducted all experiments; HIN, JMH and IC wrote the manuscript; IC and JMH secured funding and led the project.

Declaration

The authors declare no competing interests.

Data and materials availability

All data are available in the main text or the supplementary materials.

References

1. Chacinska, A., et al., *Importing Mitochondrial Proteins: Machineries and Mechanisms.* Cell, 2009. **138**(4): p. 628-644.
2. Tucker, K. and E. Park, *Cryo-EM structure of the mitochondrial protein-import channel TOM complex at near-atomic resolution.* Nature Structural & Molecular Biology, 2019. **26**(12): p. 1158-+.
3. Harbauer, A.B., et al., *The Protein Import Machinery of Mitochondria-A Regulatory Hub in Metabolism, Stress, and Disease.* Cell Metabolism, 2014. **19**(3): p. 357-372.
4. Bar-Ziv, R., T. Bolas, and A. Dillin, *Systemic effects of mitochondrial stress.* Embo Reports, 2020. **21**(6): p. 15.
5. Needs, H.I., et al., *Interplay between Mitochondrial Protein Import and Respiratory Complexes Assembly in Neuronal Health and Degeneration.* Life-Basel, 2021. **11**(5).
6. Sokol, A.M., et al., *Mitochondrial protein translocases for survival and wellbeing.* Febs Letters, 2014. **588**(15): p. 2484-2495.
7. Schon, E.A. and S. Przedborski, *Mitochondria: The Next (Neurode)Generation.* Neuron, 2011. **70**(6): p. 1033-1053.
8. Lin, M.T. and M.F. Beal, *Mitochondrial dysfunction and oxidative stress in neurodegenerative diseases.* Nature, 2006. **443**(7113): p. 787-795.
9. Devi, L., et al., *Accumulation of amyloid precursor protein in the mitochondrial import channels of human Alzheimer's disease brain is associated with mitochondrial dysfunction.* Journal of Neuroscience, 2006. **26**(35): p. 9057-9068.
10. Yano, H., et al., *Inhibition of mitochondrial protein import by mutant huntingtin.* Nature Neuroscience, 2014. **17**(6): p. 822-831.
11. Tapia-Rojas, C., et al., *It's all about tau.* Progress in Neurobiology, 2019. **175**: p. 54-76.
12. Witman, G.B., et al., *TUBULIN REQUIRES TAU FOR GROWTH ONTO MICROTUBULE INITIATING SITES.* Proceedings of the National Academy of Sciences of the United States of America, 1976. **73**(11): p. 4070-4074.
13. Binder, L.I., A. Frankfurter, and L.I. Rebhun, *THE DISTRIBUTION OF TAU IN THE MAMMALIAN CENTRAL NERVOUS-SYSTEM.* Journal of Cell Biology, 1985. **101**(4): p. 1371-1378.
14. Black, M.M., et al., *Tau is enriched on dynamic microtubules in the distal region of growing axons.* Journal of Neuroscience, 1996. **16**(11): p. 3601-3619.
15. Chaudhary, A.R., et al., *Tau directs intracellular trafficking by regulating the forces exerted by kinesin and dynein teams.* Traffic, 2018. **19**(2): p. 111-121.
16. Dixit, R., et al., *Differential regulation of dynein and kinesin motor proteins by tau.* Science, 2008. **319**(5866): p. 1086-1089.

17. Mandelkow, E.M., et al., *MARK/PAR1 kinase is a regulator of microtubuledependent transport in axons.* Journal of Cell Biology, 2004. **167**(1): p. 99-110.
18. Ebneth, A., et al., *Overexpression of tau protein inhibits kinesin-dependent trafficking of vesicles, mitochondria, and endoplasmic reticulum: Implications for Alzheimer's disease.* Journal of Cell Biology, 1998. **143**(3): p. 777-794.
19. Stamer, K., et al., *Tau blocks traffic of organelles, neurofilaments, and APP vesicles in neurons and enhances oxidative stress.* Journal of Cell Biology, 2002. **156**(6): p. 1051-1063.
20. Szabo, L., A. Eckert, and A. Grimm, *Insights into Disease-Associated Tau Impact on Mitochondria.* International Journal of Molecular Sciences, 2020. **21**(17): p. 27.
21. Barbier, P., et al., *Role of Tau as a Microtubule-Associated Protein: Structural and Functional Aspects.* Frontiers in Aging Neuroscience, 2019. **11**: p. 14.
22. Guo, T., W. Noble, and D.P. Hanger, *Roles of tau protein in health and disease.* Acta Neuropathologica, 2017. **133**(5): p. 665-704.
23. Avila, J., et al., *Role of tau protein in both physiological and pathological conditions.* Physiological Reviews, 2004. **84**(2): p. 361-384.
24. Poorkaj, P., et al., *Frequency of tau gene mutations in familial and sporadic cases of non-Alzheimer dementia.* Archives of Neurology, 2001. **58**(3): p. 383-387.
25. Goedert, M. and R. Jakes, *Mutations causing neurodegenerative tauopathies.* Biochimica Et Biophysica Acta-Molecular Basis of Disease, 2005. **1739**(2-3): p. 240-250.
26. Murakami, T., et al., *Cortical neuronal and glial pathology in TgTau(P301L) transgenic mice - Neuronal degeneration, memory disturbance, and phenotypic variation.* American Journal of Pathology, 2006. **169**(4): p. 1365-1375.
27. Li, X.C., et al., *Human wild-type full-length tau accumulation disrupts mitochondrial dynamics and the functions via increasing mitofusins.* Scientific Reports, 2016. **6**: p. 10.
28. Lasagna-Reeves, C.A., et al., *Tau oligomers impair memory and induce synaptic and mitochondrial dysfunction in wild-type mice.* Molecular Neurodegeneration, 2011. **6**: p. 14.
29. Hu, Y., et al., *Tau accumulation impairs mitophagy via increasing mitochondrial membrane potential and reducing mitochondrial Parkin.* Oncotarget, 2016. **7**(14): p. 17356-17368.
30. Cieri, D., et al., *Tau localises within mitochondrial sub-compartments and its caspase cleavage affects ER-mitochondria interactions and cellular Ca2+ handling.* Biochimica Et Biophysica Acta-Molecular Basis of Disease, 2018. **1864**(10): p. 3247-3256.
31. Chacinska, A., et al., *Mitochondrial translocation contact sites: separation of dynamic and stabilizing elements in formation of a TOM-TIM-preprotein supercomplex.* Embo Journal, 2003. **22**(20): p. 5370-5381.
32. Ford, H.C., et al., *Towards a molecular mechanism underlying mitochondrial protein import through the TOM and TIM23 complexes.* Elife, 2022. **11**.
33. Cheung, T.M.J., *A small molecule dissociates the PAM motor from the TIM23 channel*, in *Biochemistry and Molecular Biology*. 2017, University of California Los Angeles. p. 123.
34. Bittins, M. and X. Wang, *TNT-Induced Phagocytosis: Tunneling Nanotubes Mediate the Transfer of Pro-Phagocytic Signals From Apoptotic to Viable Cells.* Journal of Cellular Physiology, 2017. **232**(9): p. 2271-2279.
35. Kumar, A., et al., *Influenza virus exploits tunneling nanotubes for cell-to-cell spread.* Scientific Reports, 2017. **7**: p. 14.
36. Luchetti, F., et al., *Fas Signalling Promotes Intercellular Communication in T Cells.* Plos One, 2012. **7**(4): p. 12.
37. Grabrucker, A., et al., *Synaptogenesis of hippocampal neurons in primary cell culture.* Cell and Tissue Research, 2009. **338**(3): p. 333-341.

38. LaBarbera, K.M., et al., *Modeling the mature CNS: A predictive screening platform for neurodegenerative disease drug discovery.* Journal of Neuroscience Methods, 2021. **358**: p. 9.
39. Grubb, M.S. and J. Burrone, *Building and maintaining the axon initial segment.* Current Opinion in Neurobiology, 2010. **20**(4): p. 481-488.
40. Broadhead, M.J., et al., *PSD95 nanoclusters are postsynaptic building blocks in hippocampus circuits.* Scientific Reports, 2016. **6**: p. 14.
41. Chen, X.B., et al., *PSD-95 Is Required to Sustain the Molecular Organization of the Postsynaptic Density.* Journal of Neuroscience, 2011. **31**(17): p. 6329-6338.
42. Liu, D.L., et al., *Intercellular mitochondrial transfer as a means of tissue revitalization.* Signal Transduction and Targeted Therapy, 2021. **6**(1): p. 18.
43. Devi, L., et al., *Mitochondrial import and accumulation of alpha-synuclein impair complex I in human dopaminergic neuronal cultures and Parkinson disease brain.* Journal of Biological Chemistry, 2008. **283**(14): p. 9089-9100.
44. Pereira, G.C., et al., *A High-Resolution Luminescent Assay for Rapid and Continuous Monitoring of Protein Translocation across Biological Membranes.* Journal of Molecular Biology, 2019. **431**(8): p. 1689-1699.
45. Lei, X.H. and B.R. Bochner, *Optimization of cell permeabilization in electron flow based mitochondrial function assays.* Free Radical Biology and Medicine, 2021. **177**: p. 48-57.
46. Martin, S. and J.M. Henley, *Activity-dependent endocytic sorting of kainate receptors to recycling or degradation pathways.* Embo Journal, 2004. **23**(24): p. 4749-4759.
47. Needs, H.I., et al., *The NanoLuc Assay System for Accurate Real-Time Monitoring of Mitochondrial Protein Import within Intact Mammalian Cells.* bioRxiv, 2022: p. 2022.09.23.509159.
48. Rueden, C.T., et al., *ImageJ2: ImageJ for the next generation of scientific image data.* Bmc Bioinformatics, 2017. **18**: p. 26.
49. Schindelin, J., et al., *Fiji: an open-source platform for biological-image analysis.* Nature Methods, 2012. **9**(7): p. 676-682.
50. Cross, S. *miaanalysis/mia: Version 0.21.0*. 2021 [cited 2022 18th January].
51. Seager, R.A., *Investigating the role of SUMOylation of Mitochondrial Fission Factor in Mitochondrial Dynamics*. 2020, University of Bristol. p. 289.
52. Creed, S. and M. McKenzie, *Measurement of Mitochondrial Membrane Potential with the Fluorescent Dye Tetramethylrhodamine Methyl Ester (TMRM)*, in *Cancer Metabolism: Methods and Protocols*, M. Haznadar, Editor. 2019, Springer New York: New York, NY. p. 69-76.

Figures & Legends

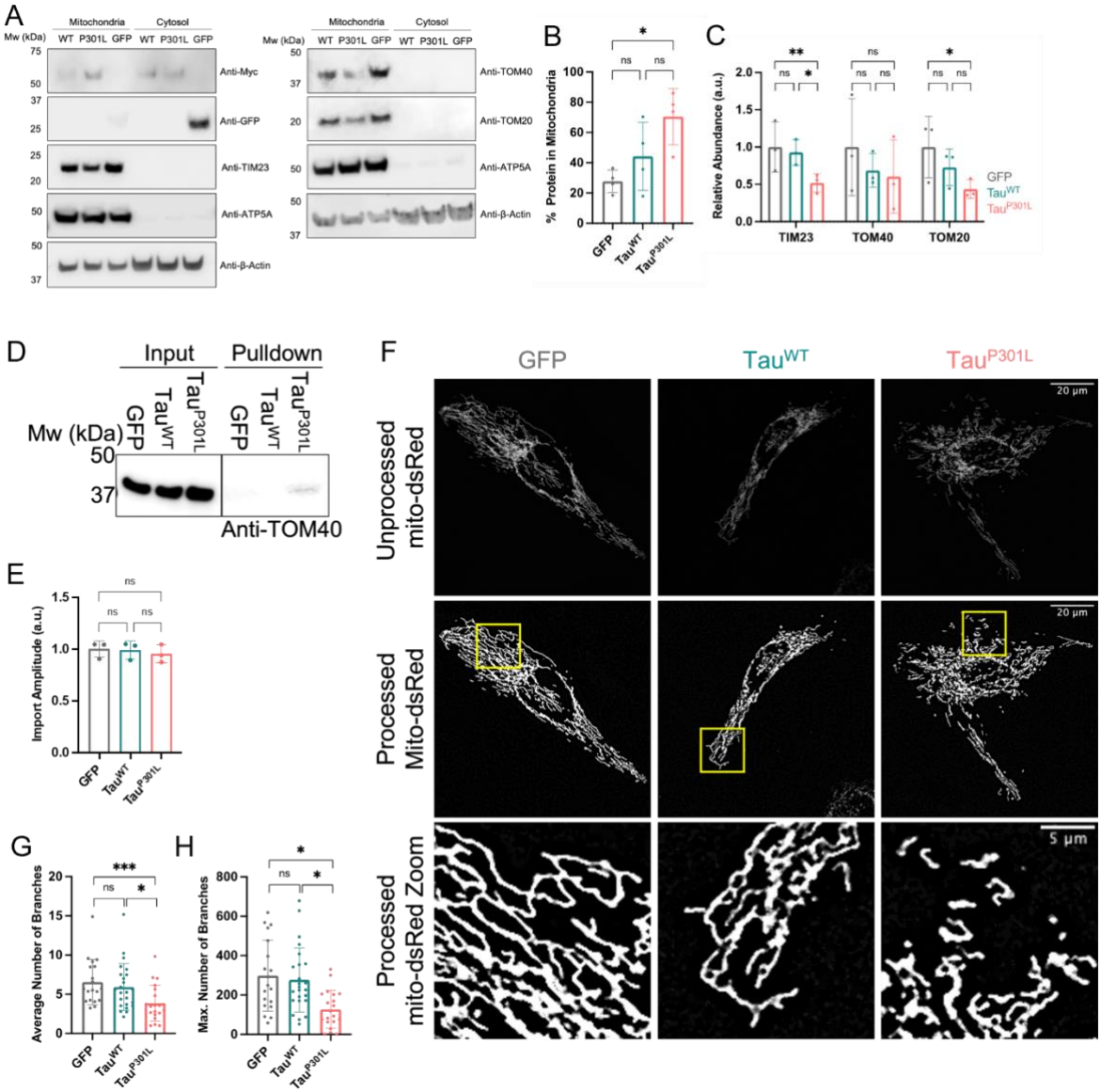

Figure 1: Tau^{P301L} Associates with the Mitochondrial Translocation Machinery and Alters Mitochondrial Morphology

(A) Western blots showing relative protein abundance in mitochondria and cytosol of HeLaGAL cells expressing GFP, Myc-Tau^{WT} and Myc-Tau^{P301L}. Localisation of GFP, Tau^{WT} and Tau^{P301L} was analysed by probing for GFP or Myc. Translocase subunits abundance was analysed by probing for TIM23, TOM40, and TOM20. ATP5A and β-actin were used as loading controls for mitochondria and cytosol, respectively. N=4 (GFP/Myc) and N=3 (translocases) biological replicates.

(B) Quantification of % GFP, Tau^{WT} or Tau^{P301L} in mitochondrial fraction. Normalised to loading controls. Error bars show SD. One-way ANOVA and Tukey's post hoc test were used to determine significance.

(C) Quantification of translocase subunits (TIM23, TOM40, TOM20). Error bars show SD. One-way ANOVA and Tukey's post hoc test were used to determine significance.

(D) Representative Western blot showing expression of TOM40 associated with Myc tagged GFP, Tau^{WT}, and Tau^{P301L}, in mitochondrial fraction of HeLaGAL cells, in input and pulldown samples. N=4 biological replicates. Control blot shown in supplementary Fig. S1.

(E) Maximum import amplitude from NanoLuc import assay. Bars represent relative maximum import of a precursor protein in HeLaGAL cells expressing GFP, Tau^{WT}, or Tau^{P301L} (normalised to eqFP670 expression, max amplitude/run, and control (GFP)). N=3 biological repeats, each with n=3 technical replicates. Error bars display SD. One-way ANOVA with Tukey's post hoc test were used to determine significance. Import trace shown in supplementary Fig. S2.

(F) Confocal microscopy showing mitochondria in HeLaGAL cells expressing mito-dsRed and GFP (left, grey), Tau^{WT} (middle, teal) or Tau^{P301L} (right, pink). The top panel shows mito-dsRed (mitochondria) prior to processing. The middle panel shows mitochondria after processing, allowing for clearer visualisation of the mitochondrial morphology. The bottom panel shows a zoom of an area of mitochondria (highlighted in the middle panel) to give a clear view of mitochondrial morphology. Representative images taken from N=5 biological repeats.

(G) Quantification of the average number of mitochondrial branches. Representative images shown in *(F)*. Each point represents an individual cell from a separate z-stack. N=20, 24, 23 for different conditions, respectively, taken from 5 independent biological repeats (N=5). Error bars show SD. Nested one-way ANOVA and Tukey's post hoc test were used to determine significance.

(H) Quantification of the maximum number of mitochondrial branches in a network. *As in (G).*

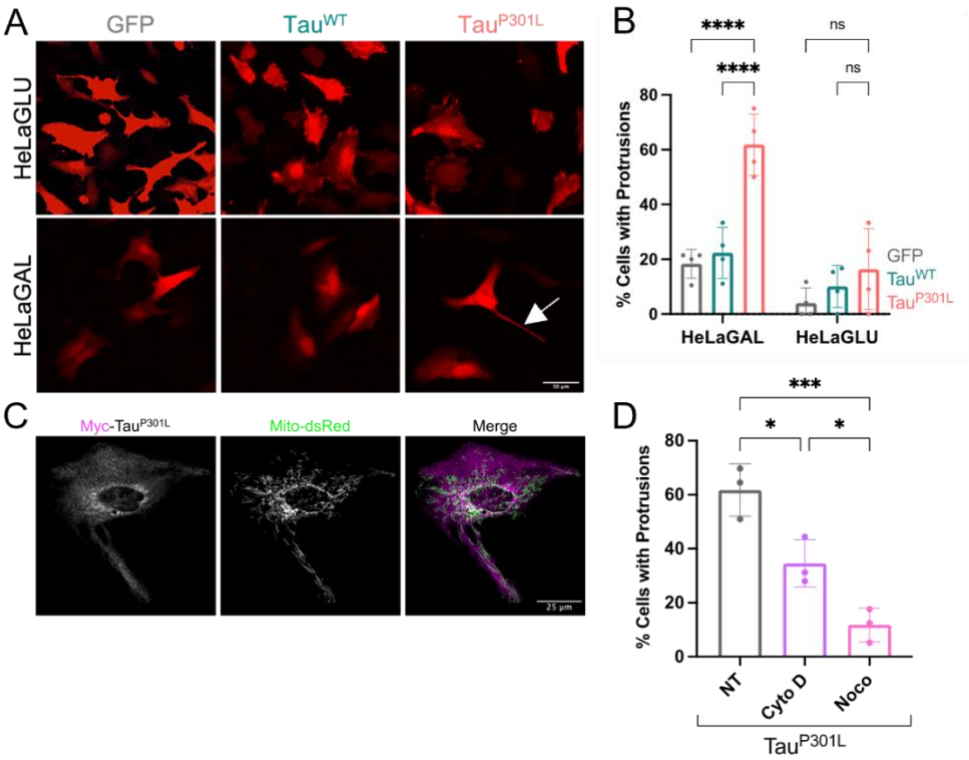

Figure 2: HeLaGAL Cells Expressing Tau^{P301L} Form TNTs that Contain Mitochondria

(A) Representative confocal images showing cell morphology of HeLaGLU or HeLaGAL cells subjected to expression of mCherry (red) as well as GFP, Tau^{WT}, or Tau^{P301L}. White arrow in bottom right panel indicates a TNT. N=4 biological replicates.

(B) Quantification of the proportion of cells with protrusions from representative images shown in *(A)*. Error bars show SD. Two-way ANOVA and Tukey's post hoc test were used to determine significance. N=4 biological replicates, 20 cells counted per replicate.

(C) Representative confocal images showing mitochondrial localisation (mito-dsRed; green) in cells overexpressing Myc-Tau^{P301L} (magenta). N=4 biological replicates.

(D) Quantification of % HeLaGAL cells with protrusions following exposure to Tau^{P301L} overexpression in the presence of TNT inhibitors. HeLaGAL cells were subjected to overexpression of Tau^{P301L}-mScarlet (green) and either untreated (NT; DMSO only) or treated with 50 nM Cytochalasin D or 100 nM Nocodazole. N=3 biological replicates, 20 cells counted per replicate. Error bars show SD. One-way ANOVA and Tukey's post hoc test were used to determine significance. Representative images shown in supplementary Fig. S5.

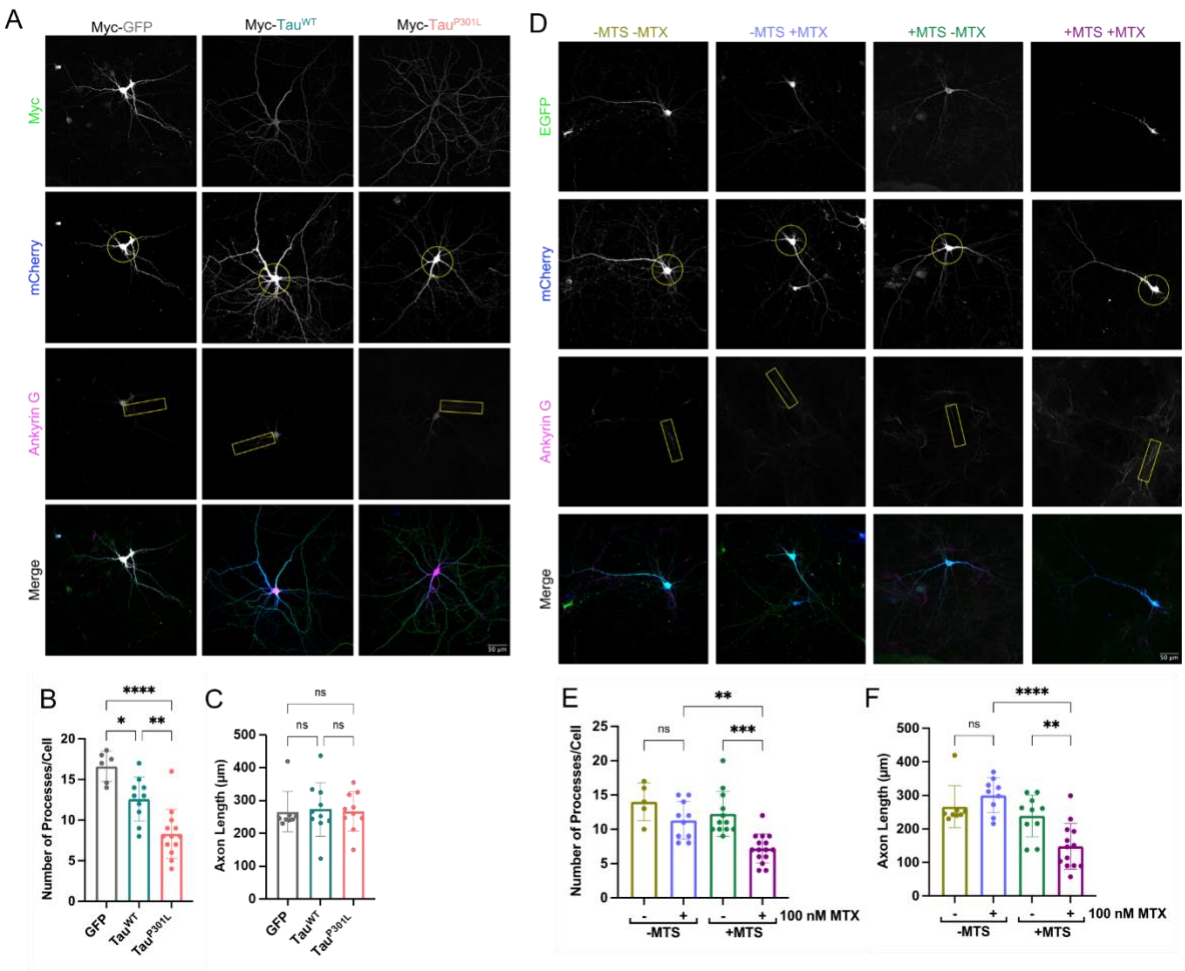

Figure 3: Tau^{P301L} Association with TOM40 Reduces Neuronal Complexity Similarly to Precursor Import Stalling

(A) Representative images showing morphology of DIV21 primary hippocampal neurons expressing mCherry (whole cell cytosolic marker; blue; circle used to highlight complexity in second panel down *i.e.,* the number of processes that cross the circle is representative of number of processes per cell) and Myc tagged GFP, Tau^{WT}, or Tau^{P301L} (Myc; green), taken by confocal microscopy. Axons were stained with Ankyrin-G (magenta; highlighted by box in third panel down). N=4 biological replicates.

(B) Quantification of number of processes per cell. Each data point represents an individual cell (cells were only analysed if the entire cell could be identified separately from surrounding cells). Error bars show SD. Nested one-way ANOVA and Tukey's post hoc test were used to determine significance.

(C) Quantification of axon length. Cells were only analysed if the axon could be clearly identified. Statistical analysis is as above.

(D) Representative confocal images showing the morphology of DIV21 primary hippocampal neurons expressing mCherry (whole cell cytosolic marker; blue; circle used to highlight complexity in second panel down *i.e.,* the number of processes that cross the circle is

representative of number of processes per cell) as well as EGFP-DHFR-HiBit (-MTS; green; top panel) or Su9-EGFP-DHFR-HiBit (+MTS; green; top panel) +/- MTX. Axons were stained with Ankyrin-G (magenta; highlighted by box in third panel down). N=5 biological replicates.

(E) Quantification of the number of processes per cell. Each data point represents an individual cell (cells were only analysed if the entire cell could be identified separately from surrounding cells). Statistical analysis as in (B).

(F) Quantification of axonal length. Cells were only analysed if the axon could be clearly identified. Statistical analysis as in (B).

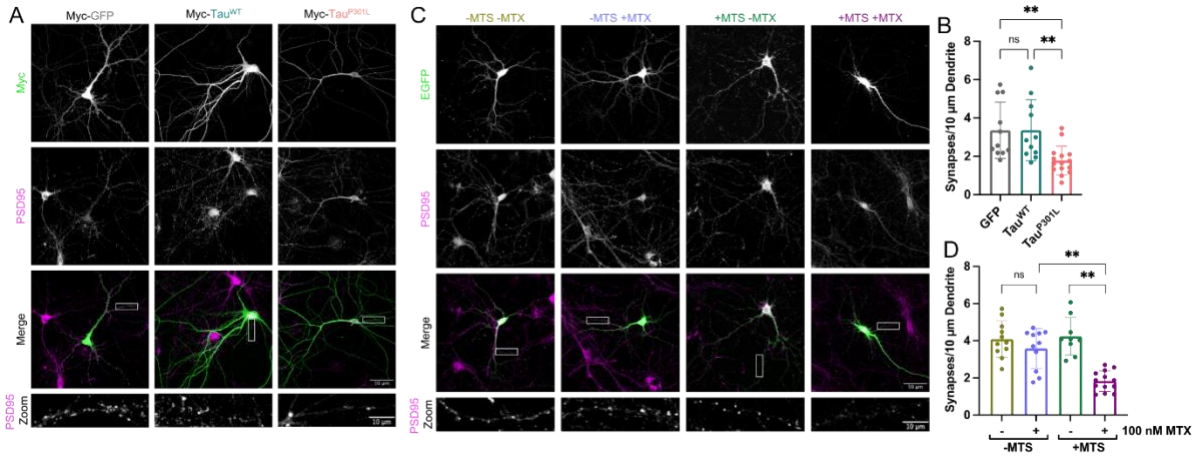

Figure 4: Precursor Trapping and Tau^{P301L} Association with TOM40 Reduce Synapse Abundance

(A) Representative confocal microscopy images showing synaptic staining of DIV21 primary hippocampal neurons expressing Myc tagged GFP, Tau^{WT}, or Tau^{P301L} (Myc; green). PSD95 staining shows synapses (magenta; second panel from top, also shown in zoom). N=5 biological replicates.

(B) Quantification of the average number of synapses per 10µm dendrite. Synapses were counted manually on blinded data. Each data point represents an individual cell. Error bars show SD. Nested one-way ANOVA and Tukey's post hoc test were used to determine significance.

(C) Representative confocal microscopy images showing synaptic staining of DIV21 primary hippocampal neurons expressing EGFP-DHFR-HiBit (-MTS) or Su9-EGFP-DHFR-HiBit (+MTS; EGFP shown in green, top panels) in the absence or presence of 100 nM MTX (-/+MTX). PSD95 staining shows synapses (magenta, second panel from top, also shown in zoom). N=5 biological replicates.

(D) Quantification of the average number of synapses per 10µm dendrite. Synapses were counted manually on blinded data. Each data point represents an individual cell. Error bars show SD. Nested one-way ANOVA and Tukey's post hoc test were used to determine significance.

Supplementary Information

Materials & Methods

Reagents

All chemicals were of the highest grade of purity commercially available and generally purchased from Sigma, UK unless stated otherwise. Aqueous solutions were prepared in ultrapure water, while for non-aqueous solutions, ethanol or DMSO was used as solvent instead.

Generation of Constructs

Constructs were generated by standard cloning techniques. Briefly, PCR reactions were carried out using Q5 High Fidelity Hot Start DNA Polymerase (New England Biolabs (NEB)), using 20 pmol primers and 200 pg template DNA, as per manufacturers' instructions. PCR products were purified using QIAquick PCR Purification Kit (QIAgen). Restriction digest reactions were carried out using NEB restriction enzymes at 37ºC for 45-60 minutes. Ligation reactions were carried out using T4 DNA Ligase (NEB) overnight at 16ºC. Transformation was carried out in *E. coli* cells (α-select, XL1-Blue, or BL21-DE3 cells were used, depending on application; all originally sourced from NEB and stored at -80ºC) for 30 min on ice, followed by heat shocking (45 seconds, 42ºC), and a further 15 min on ice. Cells were recovered by incubating in LB media at 37ºC for 1 hour and then plated on LB-agar plates containing appropriate antibiotic. Plasmids were prepared by mini or maxi preps using commercially available kits (Qiagen and Promega, respectively) following manufacturers' instructions, and verified by DNA sequencing using Eurofins Genomics TubeSeq service.

Protein Purification

Protein expression was carried out exactly as described previously [44]. A single colony of transformed BL21 (DE3) bacteria was grown as a pre-culture in LB with appropriate antibiotic overnight (37°C; 200 rpm). Pre-cultures were used to inoculate a secondary culture at a 1:100 dilution, in 2X YT supplemented with appropriate antibiotic. Secondary cultures were grown until mid-log phase, then induced with 1 mM IPTG or 0.2% (w/v) Arabinose and grown for a further 3 h. Cells were harvested by centrifugation (15 min; 6000 xg), resuspended in TK buffer (20 mM TRIS base, 50 mM KCl; pH 8.0), cracked in a cell disruptor (Constant Systems; 2 cycles at 25 kpsi), and clarified by centrifugation (45 min; 38,000 rpm).

GST tagged Recombinant Perfringolysin (rPFO)

Supernatant (soluble fraction) was loaded onto a 5 mL GSTrap 4B column (GE Healthcare) and the column was washed with TK buffer until the absorbance of the flow through ceased to decrease any further. The peptide was eluted using 10 µM reduced glutathione, prepared fresh. Eluted fractions were pooled and loaded onto a 5 ml anionic exchanger (Q- column; GE Healthcare). A salt gradient of 0-1 M was applied over 20 min and the protein was eluted in 5 ml fractions. The fractions containing the protein were confirmed by SDS-PAGE with Coomassie staining, then pooled and spin concentrated. The final protein concentration was determined based on an extinction coefficient of 117,120 M^{-1} cm^{-1}. The protein was aliquoted, snap frozen, and stored at -80°C until required. For each assay, a fresh aliquot was thawed, used immediately, and discarded afterwards, due to the instability of this protein [45].

GST-Dark Peptide

GST-Dark was prepared as described previously [44]. Supernatant was loaded onto a GSTrap 4B column and purification was carried out exactly as for rPFO but without the ion exchange chromatography. Analysis, yield, and freezing was carried out exactly as for rPFO. Protein concentration was determined based on an extinction coefficient of 48,360 M^{-1} cm^{-1}.

His tagged Su9-EGFP-pep86

Inclusion bodies (insoluble fraction) were solubilised in TK buffer supplemented with 6 M urea, before loading onto a 5 ml HisTrap HP column (GE Healthcare). The protein was eluted in 300 mM imidazole. Eluted fractions containing the desired protein were pooled and loaded onto a 5 ml cationic exchanger (S- column; GE Healthcare). A salt gradient of 0-1 M was applied over 20 min and the protein was eluted in 5 ml fractions. Imidazole was removed by spin concentration, followed by dilution in TK buffer containing 6 M urea. Analysis, yield, and freezing were carried out exactly as for rPFO. Protein concentration was determined based on an extinction coefficient of 28,880 M^{-1} cm^{-1}.

Cell Culture

HeLa/HEK293T Cell Culture

HEK293T (ECACC) and glucose-grown HeLa cells (HeLaGLU; ATCC) were maintained in Dulbecco's Modified Eagle's Medium (DMEM; Gibco; 41965039) supplemented with 10% (v/v) foetal bovine calf serum (FBS; Invitrogen) and 1% (v/v) penicillin-streptomycin (P/S; Invitrogen). When OXPHOS dependence was required, HeLa cells were cultured in galactose medium (HeLaGAL; ATCC) consisting of DMEM without glucose (Gibco; 11966025) supplemented with 10 mM galactose, 1 mM sodium pyruvate, 10% FBS and 1% P/S. Cells

were cultured in galactose media for at least 3 weeks prior to experiments on HeLaGAL cells. Cells were maintained in T75 ventilated flasks in humidified incubators at 37ºC with 5% CO_2.

Primary Neuronal Cell Culture

Primary neuronal culture was carried out following established lab protocols, as described previously [46]. Briefly, primary hippocampal and cortical neurons were isolated from embryonic day 18 (E18) Han Wistar rat pups. Pregnant Han Wistar rats, bred in-house at the University of Bristol Animal Services Unit, were anaesthetised using isoflurane with pure oxygen flow and humanely killed by means of cervical dislocation, following Home Office Schedule 1 regulations. Isolated neurons were washed extensively in HBSS and dissociated by incubation with 10% (v/v) Trypsin-EDTA solution at 37ºC for 15 or 9 min, for cortical or hippocampal neurons, respectively. Cells were grown in plating medium (Neurobasal medium (Gibco) supplemented with 10% (v/v) horse serum (Sigma), 2% (v/v) B27 (Gibco), 1% P/S, and 5 mM Glutamax (Gibco)). After 2-3 hours, plating medium was removed and replaced with feeding medium (Neurobasal medium supplemented with B27, P/S, and 2 mM Glutamax). For biochemistry, cortical neurons were seeded at a density of 500,000 cells per well and for imaging experiments, hippocampal neurons were seeded at a density of 100,000 cells per well, where one well represents a ~35 mm surface. All plates (containing sterile coverslips if appropriate) were incubated with poly-L-lysine (0.5 mg/ml or 1 mg/ml for plastic or glass, respectively, in sterile borate buffer (1 mM borax and 5 mM boric acid)) overnight, extensively washed with tissue culture grade H_2O and incubated overnight in plating medium prior to plating cells, to aid adhesion. Cells were maintained in humidified incubators at 37ºC with 5% CO_2.

Transfection of Cells

HeLa Cell Transfection

HeLa cells were plated and grown up to 70-80% confluency. At this point cells were transfected with 1 µg (per 35mm dish) of the desired DNA using Lipofectamine 3000 reagent (Thermo Fisher Scientific), at a 1:1.5 ratio of DNA:Lipofectamine, following the manufacturers' protocol. Cells were then grown for a further 24-72 h prior to experimental analysis.

Primary Neuron Transfection

Primary neurons were transfected at 14 days *in vitro* (DIV14) with 0.5-1 µg of the desired DNA using Lipofectamine 2000 reagent (Thermo Fisher Scientific), at a ratio of 1.5 µl Lipofectamine 2000 per 1 µg DNA. Coverslips with adhered neurons were washed in plain neurobasal medium and transferred to dishes containing 1 ml plain neurobasal medium, to which the transfection mix was added. 45 min after transfection, coverslips were washed again to

remove all remaining DNA and Lipofectamine 2000 from cells and returned to their conditioned growth medium. Neurons were then maintained for a further 7 days prior to fixation.

Cell Transduction by Lentiviral Infection

Lentiviral particles were produced in HEK293T cells by addition of a mixture of DNAs (27.2 µg DNA to be produced, and packaging vectors pMDG2 (6.8 µg) and pAX2 (20.4 µg)) and 1 µg/µl pEI transfection reagent in OptiMEM medium (Gibco) to HEK293T cells in a T75 flask, followed by incubation for 6 hours at 37ºC, 5% CO_2. Media was then changed to complete DMEM, and cells incubated for 72 h to allow lentivirus particle production. Lentivirus particles were harvested at 48 and 72 h for maximum yield, pooled, spun down at 4000 xg for 5 min to remove dead cells, and concentrated by adding Lenti-X concentrator (Takara Bio) at a 1:3 ratio and incubating at 4ºC for at least 1 h. Lentivirus was then pelleted by centrifugation at 4000 xg for 45 min. Pellets were resuspended in plain DMEM at 1:50 of initial supernatant volume and aliquoted and stored at -80ºC until required. For infection, concentrated lentivirus (volume optimised by titration of each fresh batch) was added dropwise to cell media and cells incubated prior to experimental analysis (see figure legends for details of incubation times).

Mitochondrial Isolation

Confluent cells were harvested by trypsinisation, pelleted, and washed extensively with HBSS. Pellets were frozen overnight at -80ºC and thawed the next day, to weaken membranes. Subsequently, mitochondrial isolation was performed using Mitochondrial Isolation Kit for Cultured Cells (Abcam; ab110170) following manufacturers' instructions. Mitochondrial protein concentration was calculated using BCA assays using BSA as a standard.

Immunoprecipitation

Following mitochondrial isolation, mitochondria were gently lysed using 4.5 g GDN/ g protein in IP buffer (0.1M TrisHCl, 0.15M NaCl, phospholipids (0.03 mg/ml PE; 0.03 mg/ml PG; 0.09 mg/ml PC), 1X cOmplete ULTRA Protease Inhibitor Cocktail). Myc-tagged proteins were isolated using 10 µl Myc-Trap beads (Chromotek). Supernatant (lysed mitochondrial sample) was incubated on a rotating wheel with beads overnight at 4ºC. Subsequently, beads were washed in IP buffer. After washing, supernatant was removed, and samples were analysed by Western blotting.

Total Protein Cell Lysis

For extraction of total protein lysate, cells were washed extensively with HBSS, and RIPA buffer (Sigma, supplemented with 1 mM PMSF) was added (200 µl for ~35 mm surface, scaled up or down appropriately). Cells were scraped on ice into Eppendorf tubes, which were

incubated for 1 h on a rotating wheel at 4°C, prior to spinning down at 10,000 xg for 15 min at 4°C. Supernatant (containing proteins) was stored at -20°C. Protein concentration was obtained by carrying out a BCA assay (Pierce™ BCA Protein Assay Kit, Thermo Fisher Scientific), following manufacturer's instructions and using BSA as a standard.

Western Blotting

Following total protein extraction, protein samples were heated to 95°C for 5 min in the presence of LDS supplemented with 50 mM DTT. 30 µg of total protein was loaded on 4-12% BOLT gels (Thermo Fisher Scientific), separated (200 V, 24 min), and transferred onto polyvinylidene difluoride (PVDF) membranes (activated with methanol; Thermo Fisher Scientific) with transfer buffer (336 mM tris, 260 mM glycine, 140 mM tricine, 2.5 mM EDTA) using a semi-dry Pierce Power Station transfer system (Thermo Fisher Scientific; 2.5 mAmp, 10 min). Membranes were blocked for 1 h in milk (5% w/v in TBS-T: 20 mM TRIS, 1.5 M NaCl, 0.1% (v/v) Tween-20 (pH 7.6)) and incubated in 5% milk containing the appropriate primary antibody (4°C, overnight). Membranes were washed extensively with TBS-T and probed with appropriate secondary antibody in 2.5% milk (RT, 1 hour). Membranes were washed with TBS-T, incubated with ECL substrate (GE Healthcare), and developed using an Odyssey Fc Imaging System (LI-COR). Analysis and quantification were carried out using Image Studio Lite software.

NanoLuc Assay

NanoLuc assays were carried out exactly as described previously [47]. Briefly, cells on standard white flat-bottom 96-well plates were washed with HBSS wash buffer (HBSS supplemented with 5 mM D-(+)-glucose, 10 mM HEPES (Santa Cruz Biotechnology, Germany), 1 mM $MgCl_2$, 1 mM $CaCl_2$; pH 7.4). A fluorescence read was taken at 605/670 nm using monochromators with gain set to allow maximum sensitivity without saturation, using a BioTek Synergy Neo2 plate reader. Cells were transferred to permeabilised cell assay master mix (225 mM mannitol, 10 mM HEPES, 2.5 mM $MgCl_2$, 40 mM KCl, 2.5 mM KH_2PO_4, 0.5 mM EGTA; pH 7.4) supplemented with 5 mM succinate, 1 µM rotenone, 0.1 mg/ml creatine kinase, 5 mM creatine phosphate, 1 mM ATP, 0.1% (v/v) Prionex, 3 nM rPFO (purified in house), 20 µM GST-Dark (purified in house), 1:800 furimazine (Nano-Glo® Luciferase Assay System; Promega). A baseline read of 30 seconds of background luminescent signal was taken prior to injection of purified substrate protein (*Su9-EGFP-pep86*) to 1 µM final concentration, followed by a further bioluminescence read corresponding to import, lasting 30 min. Bioluminescence was read using a BioTek Synergy Neo2 plate reader (Agilent, UK) or a CLARIOstar Plus plate reader (BMG LabTech, UK) without emission filters with gain set to

allow maximum sensitivity without saturation, and with acquisition time of 0.1 sec per well. Row mode was used, and reads were taken every 6 sec or less, with wells in triplicate.

Confocal Microscopy

Fixed Cell Confocal Microscopy

Cells on glass coverslips were washed in HBSS and fixed in 4% (v/v) paraformaldehyde (PFA) with 2% (w/v) sucrose (sucrose used for neurons only, to retain osmolarity), for 12 min at 37°C. Coverslips were then washed extensively in HBSS, and PFA was quenched using 100 mM Glycine. Cells were then stained for ICC or mounted.

For immunocytochemistry, following fixation and quenching, cells were permeabilised by incubation in 0.1% (v/v) Triton-X in PBS for 5 min, washed in PBS and blocked in 3% (w/v) BSA in PBS for 30 min. Coverslips were incubated on a drop of primary antibody in 3% BSA overnight at 4°C. Coverslips were washed extensively in PBS and incubated with the appropriate secondary antibody (2 hours, RT) in 3% BSA, then washed again.

Coverslips were dipped in dH2O and mounted using Fluoromount-G mounting medium (Thermo). Coverslips were left to dry overnight and imaged using a Leica confocal microscope (SP5II or SP8) and LAS X software platform. Laser lines used were 405, 488, 562, and 633 nm, with gain set to allow maximum sensitivity without saturation, and z-stacks were taken.

Live Cell Confocal Microscopy

Transfected cells were grown to confluency on 35 mm glass bottomed dishes (Corning). Cells were washed in HBSS and incubated in imaging buffer (HBSS supplemented with 5 mM Glucose, 10 mM HEPES, 1 mM $MgCl_2$, 1.26 mM $CaCl_2$) with 25 nM tetramethylrhodamine (TMRM) for 30 min at 37°C. Cells were imaged immediately, with TMRM retained in the buffer, using a Leica SP8 confocal microscope and LAS X software platform, at 37°C.

Image Analysis

All image analysis was performed using the FiJi image processing package [48, 49]. All macros were written by Dr Stephen Cross (Wolfson Bioimaging Facility, University of Bristol), within the FiJi plugin Modular Image Analysis (MIA) package version 0.21.0, which is publicly accessible on GitHub with a linked version specific DOI from Zenodo [50]. Where data was analysed manually, data was randomised/blinded by a colleague prior to manual analysis.

Mitochondrial Morphology Analysis

Mitochondrial pre-processing, as well as branch and network analysis, was carried out using the Mitochondrial Network Analysis MiNa plugin, exactly as described previously [51]. Auto-thresholding was carried out during the pre-processing stage using Huang2 method.

Membrane Potential Analysis

TMRM analysis of mitochondrial membrane potential was done based on a published protocol [52]. Briefly, an average of the first 10 frames (TMRM fluorescence where images were captured by live confocal microscopy over 2 minutes) was taken, then the mitochondria were thresholded and their intensity measured. The average of the final three frames (after carbonyl cyanide m-chlorophenylhydrazone (CCCP) treatment to dissipate the $\Delta\Psi$) was subtracted as a control and the intensity of the subtracted image was re-measured.

Neuronal Morphology Analysis

Analysis of neuronal complexity (number of processes, *i.e.,* axon and dendrites) was carried out by manually counting the number of processes protruding from the soma (at a given distance from the soma – highlighted by circles on images). This was carried out on blinded data, where expression of the protein of interest had been confirmed (prior to data blinding) and all processes were highlighted using an mCherry cytosolic marker.

Axons in transfected cells were identified using an Ankyrin G stain. Following identification of the axon to be measured, the length of the axon was measured by tracing the length of the axon, highlighted by the mCherry cytosolic stain, using the Simple Neurite Tracer (SNT) component of the Neuroanatomy plugin in FiJi. Synapses were counted manually. First, data was blinded, and dendrites were identified. The dendrite of interest was measured using the SNT plugin and the synapses along the region of interest were counted manually using the PSD95 stain as reference. A total of 5 dendrites were analysed per cell and an average was taken for each cell.

Seahorse Assays: Mitochondrial Stress Test

Cells were seeded in 6-well plates (200,000 cells/well) and infected with the appropriate lentivirus, as described in figure legends. The day prior to the assay, cells were detached by trypsinisation, counted, and seeded at 10,000 cells/well in 96 well Seahorse XF cell culture plates (Agilent, UK). The sensor cartridges were hydrated overnight with tissue culture grade H_2O in a non-CO_2 incubator at 37°C as per manufacturer's instructions. On the day of the assay, H_2O in the sensor plate was replaced with Seahorse XF Calibrant (Agilent) and cells were washed with HBSS and incubated in Seahorse media (Seahorse XF assay medium (Agilent), 1 mM pyruvate (Agilent), 2 mM glutamine (Agilent), 10 mM D-(+)-galactose). Both

sensor and cell plates were incubated in a non-CO_2 incubator at 37°C for 1 h prior to the assay. The sensor plate was loaded with oligomycin (15 µM for 1.5 µM final concentration in wells; injector A), CCCP (5 µM for 0.5 µM final; injector B), and antimycin A and rotenone (5 µM/5 µM for 0.5 µM/0.5 µM final; injector C). The sensor plate was calibrated prior to loading cells and running a mitochondrial stress test using a Seahorse XFe96 (Agilent). Following assays, cells were washed and fixed in 1% acetic acid in methanol at -20°C overnight for SRB assays, which were used for normalising data to protein content.

SRB Assay

Cells were fixed with ice cold 1% (v/v) acetic acid in methanol overnight at -20°C. Fixative was aspirated and plates were allowed to dry at 37°C. SRB (0.5% (w/v) in 1% (v/v) acetic acid in dH_2O) was incubated in wells (37°C, 30 min). SRB was then aspirated, and unbound stain removed by washing 4 times with 1% acetic acid, prior to drying plates at 37°C. Bound protein stain was solubilised by shaking incubation with 10 mM Tris (pH 10; 15 min, RT). Absorbance was read on a microplate reader with a 544/15 nm filter.

Statistical Analysis

Statistical significance between groups was determined using unpaired Student's t-Test or one and two-way ANOVA with interaction if more than two groups were analysed. ANOVA was nested if multiple objects were analysed per biological replicate. Following ANOVA, p values were adjusted for multiple comparisons through Tukey's or Dunnett's post-hoc test and differences were considered significant at 5% level. Statistical analyses were performed using Graph Pad Prism version 9 (GraphPad Software, Inc., San Diego, CA, USA).

Supplementary Figures

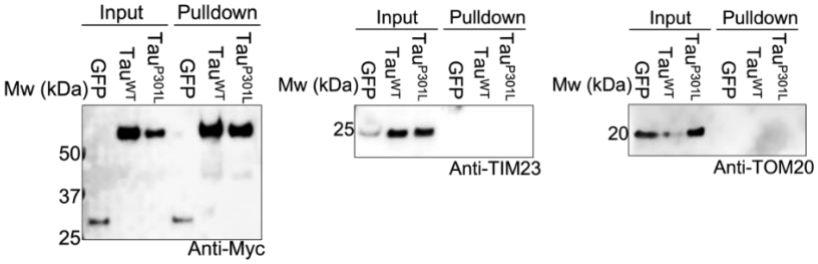

Fig. S1.

Representative Western blot showing levels of Myc (showing pulldown worked), as well as TIM23 and TOM20 in in input and pulldown samples from the mitochondrial fraction of HeLaGAL cells overexpressing Myc tagged GFP, Tau^{WT}, and Tau^{P301L}. Corresponding to IP experiment shown in Fig. 1D. N=4 biological replicates.

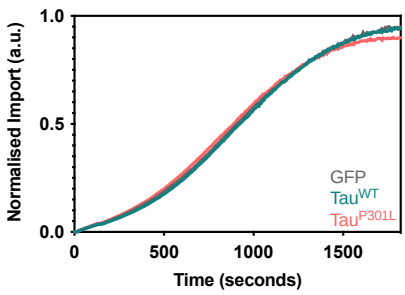

Fig. S2.

NanoLuc import assay trace showing import of a precursor protein in HeLaGAL cells expressing GFP, Tau^{WT}, or Tau^{P301L}. Averaged, normalised traces are shown (normalised to eqFP670 expression and max amplitude/run), error bars represent SD. N=3 biological repeats, each with n=3 technical replicates. Corresponds to quantification of import amplitude shown in Fig. 1E.

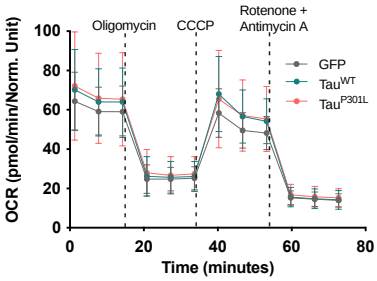

Fig. S3.

Mitochondrial stress test showing OCR of HeLaGAL cells expressing Myc-GFP, Myc-Tau^{WT}, or Myc-Tau^{P301L}. Data is normalised to protein content as determined by SRB assays. Error bars show SD. N=6 biological replicates, each with n=3 technical replicates.

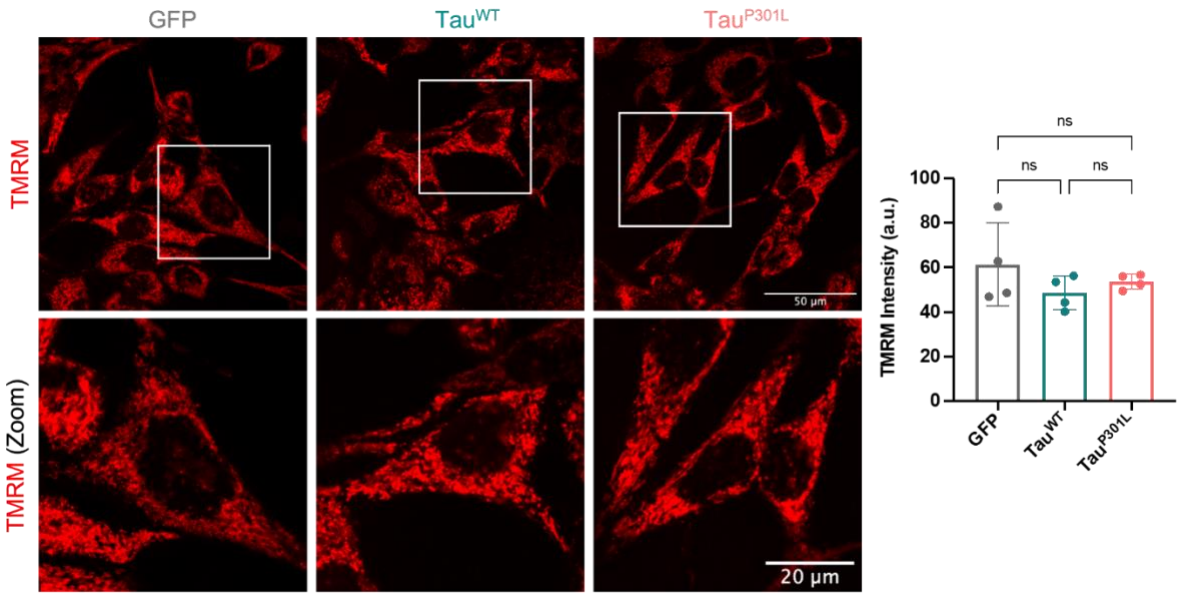

Fig. S4.

Representative confocal images showing TMRM fluorescence (red) in the mitochondria of HeLaGAL cells expressing Myc-GFP, Myc-Tau^{WT}, or Myc-Tau^{P301L}. CCCP was added after 2 minutes to control for background fluorescence. N=4 biological replicates. Right panel shows quantification of TMRM intensity. Analysis was carried out using a macro on FiJi (see Methods). Error bars show SD. One-way ANOVA and Tukey's post hoc test were used to determine significance.

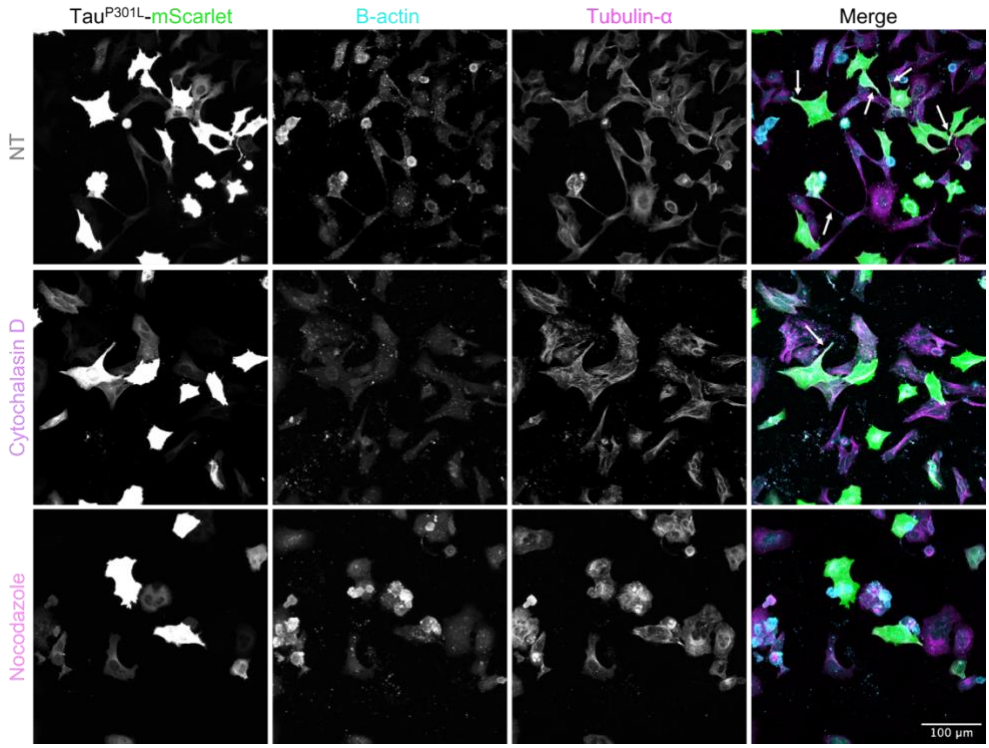

Fig. S5.

Representative images of HeLaGAL cells exposed to Tau^{P301L} overexpression in the presence of TNT inhibitors. HeLaGAL cells were subjected to overexpression of Tau^{P301L}-mScarlet (green) and either untreated (NT; DMSO only) or treated with 50 nM Cytochalasin D or 100 nM Nocodazole. Cells were fixed and stained for β-actin (cyan) and tubulin-α (magenta). Arrows in merge highlight TNTs. N=3 biological replicates. Quantification shown in Fig. 2D.

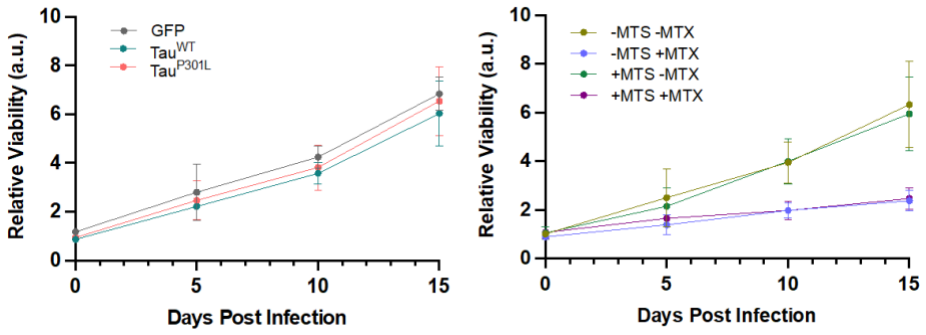

Fig. S6.

Viability of primary cortical neurons expressing GFP (control), Tau^{WT} or Tau^{P301L} (right panel), or EGFP-DHFR-HiBit (-MTS) or Su9-EGFP-DHFR-HiBit (+MTS) +/- MTX (left panel), as determined by cell density, quantified by SRB assays. Data was normalised to the average reading for the 0 days post infection timepoint, to give relative viability of the neurons in response to the varying expression/treatment. N=4 biological replicates. Error bars show SD.

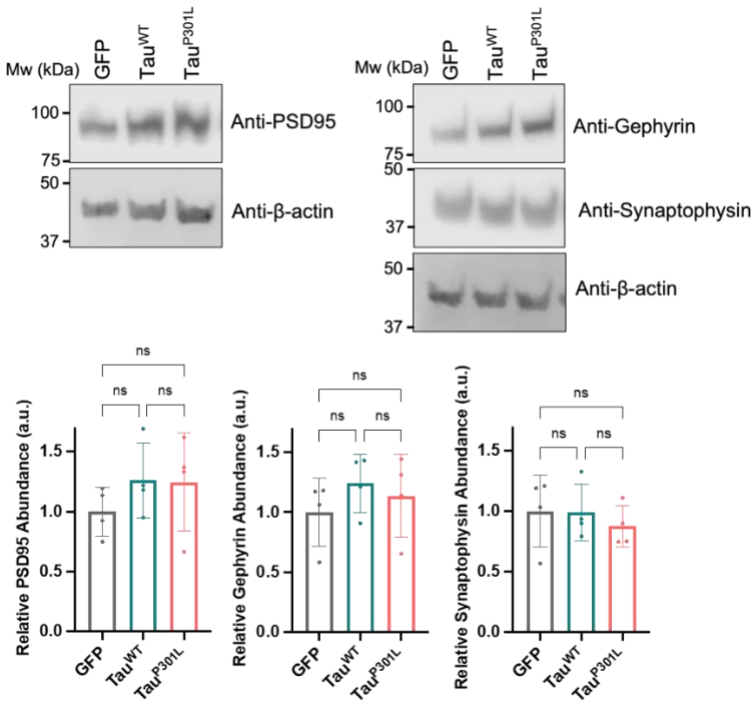

Fig. S7.

Representative Western blots showing levels of PSD95, Gephyrin, and Synaptophysin in DIV21 cortical neurons after 7 days of expression of Myc-GFP, Myc-Tau^{WT}, or Myc-Tau^{P301L}. β-actin was used as a loading control. N=4 biological replicates. Histograms show quantification of PSD95, Gephyrin, and Synaptophysin relative abundance, normalised to β-actin. Error bars show SD. One-way ANOVA and Tukey's post hoc test were used to determine significance.

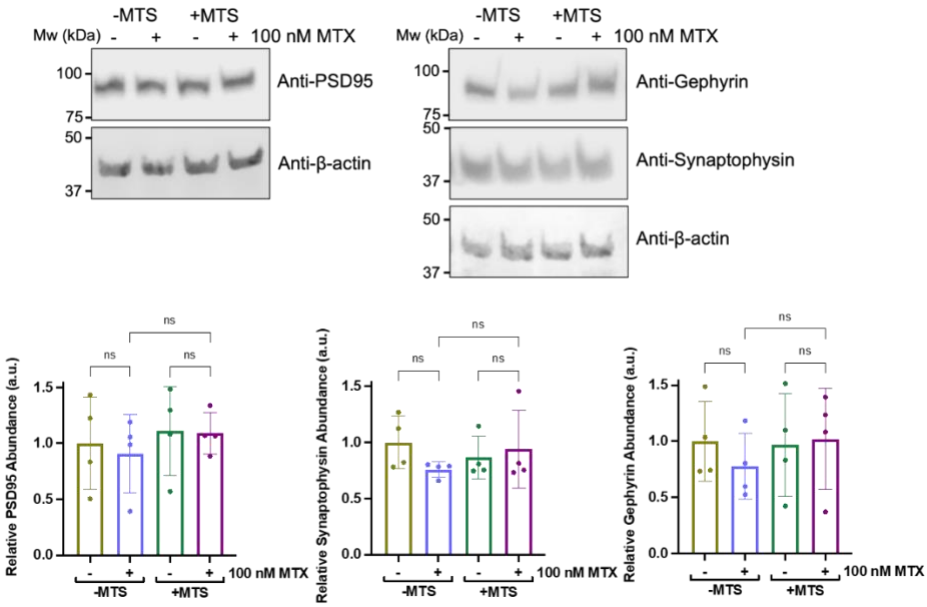

Fig. S8.

Representative Western blots showing total cellular abundance of PSD95, Gephyrin, and Synaptophysin in DIV21 cortical neurons after 7 days of expression of EGFP-DHFR-HiBit (-MTS) or Su9-EGFP-DHFR-HiBit (+MTS) +/- MTX. β-actin was used as a loading control. N=4 biological replicates. Histograms show quantification of PSD95, Gephyrin, and Synaptophysin relative abundance, normalised to β-actin. Error bars show SD. One-way ANOVA and Tukey's post hoc test were used to determine significance.